

## 1 Finite element nonlinear analysis of high-rise unreinforced masonry building

### Abstract

A simple efficient algorithm based on compressive diagonal strength of unreinforced masonry walls is presented to determine capacity curve of unreinforced masonry building. The compressive strength is calculated based on a new close form solution. The new close form solution is determined based on predicted results using interface elements for modeling of mortar joints. Finite element method with two-noded linear elements is used for analyses. Different masonry structures, including low- and high-rise unreinforced masonry buildings, are analyzed using the new closed-form solution and the presented algorithm. A comparison of results of the present work with experimental data and other methods similar to the discrete element method show proper accuracy of the analyses in the present work. Consequently, the closed form solution with proposed algorithm can be used to satisfactorily analyze unreinforced masonry structures to predict the ultimate base shear force and the pushover curve. Hence, practicing engineers can determine the behavior of an URM building and its performance level with proper accuracy under seismic excitation using concepts described in the present work.

### Keywords

Masonry wall, interface element, micro-modeling, macro-modeling, old masonry building, high-rise URM building.

**A.H. Akhaveissy\***

\* Department of Civil Engineering, Faculty Engineering, Razi University, P.O. Box: 67149-67346, Kermanshah, Iran  
Tel.: +98 831 427 4535; fax: +98 831 428 3264

Received 07 Oct 2011;  
In revised form 10 May 2012

\* Author email: [Ahakhaveissy@razi.ac.ir](mailto:Ahakhaveissy@razi.ac.ir)

## 2 1 INTRODUCTION

3 Masonry is the oldest building material that still finds wide use in today's building industries.  
4 Important new developments in masonry materials and applications have occurred in the  
5 past two decades. Masonry is a composite material that consists of units and mortar joints.  
6 Masonry buildings are constructed in many parts of the world where earthquakes occur. Hence,  
7 knowledge of their seismic behavior is necessary to evaluate the seismic performance of these  
8 types of building. Pushover analysis is commonly used to evaluate seismic performance and  
9 to determine the capacity curve. Therefore, the capacity curve is studied in this paper.

10 An approach for analysis of unreinforced masonry buildings is the macro-modeling of ma-  
11 sonry as a composite material. The macro modeling is more practice oriented due to the reduce  
12 time and memory requirements as well as a user-friendly mesh generation. The compressive  
13 strength of a masonry unit is an important parameter in the analysis of unreinforced masonry  
14 buildings using the macro-element method. A masonry unit includes mortar joints and ma-  
15 sonry bricks. The compressive strength for masonry units with different mortar was evaluated  
16 [10, 15, 16, 37, 38].

17 SAP2000 v.10, a software package with a user-friendly interface that is widely used by  
18 practicing engineers, was used for the seismic analyses of masonry buildings [31]. Two unrein-  
19 forced stone masonry walls in the Catania Project were modeled with SAP2000 v.10. The static  
20 pushover curves from the analyses were compared with predicted results from the SAM code,  
21 which was developed by the University of Pavia, the Genoa research group and the Basilicata  
22 research group [31]. The Basilicata research group used a no-tensile-strength macro-element  
23 model with crushing and shear failures while the Genoa research group used a finite element  
24 model with layer failures. The ultimate base shear force for wall A is predicted to be 1682 kN  
25 by the Genoa R.G., 1339 kN by SAP2000, 1115 kN by the SAM code, and 1395 kN by the  
26 Basilicata R.G. Accordingly, the ultimate base shear force for wall B is predicted to be 650 kN  
27 by the Genoa R.G., 474 kN by the SAM code and SAP 2000, and 508 kN by the Basilicata  
28 research group. These results show differences between the different studies. Hence, practicing  
29 engineers may be confused as to which codes or research is the most applicable or precise.

30 The in-plane shear behavior of hollow brick masonry panels was evaluated [14]. The non-  
31 linear behavior of masonry was modeled assuming elastic-perfectly plastic behavior, Drucker-  
32 Prager, of the mortar joint in the ANSYS 5.4 commercial software. In other words, the micro-  
33 element method was used to analyze the panels. A comparison between the experimental  
34 results and numerical analysis shows good agreement.

35 A macro-element approach to the three-dimensional seismic analysis of masonry buildings  
36 was applied [5]. The full model displays a base shear force that is approximately 25% higher  
37 than the value calculated for the plane structure.

38 Seismic fragility of an unreinforced masonry low-rise building was studied using a structural  
39 modeling method. The method utilizes a simple, composite nonlinear spring. In this method,  
40 the wall is divided into distinct areas or segments. Each segment of the unreinforced masonry  
41 wall is then represented by a nonlinear spring, and the springs are assembled in series and in  
42 parallel to match the segment topology of the wall [30]. Rota et al.[33] presented a new ana-  
43 lytical approach for the derivation of fragility curves for masonry buildings. The methodology  
44 was based on nonlinear stochastic analyses of building prototypes. Monte Carlo simulations  
45 were used to generate input variables from the probability density functions of mechanical  
46 parameters.

47 The seismic performance of existing unreinforced masonry buildings in North America were  
48 considered in a state-of-the-art paper [7]. The various failure modes of unreinforced masonry  
49 buildings subjected to earthquake excitation were described in the paper. The damage to the  
50 existing buildings for different earthquake scenarios was evaluated.

51 The static pushover curve was studied using the boundary element method for unreinforced  
52 masonry walls [3]. In the analysis, a no-tension-material with an infinite strength in compression  
53 was adopted to model the masonry buildings. The predicted results show good agreement  
54 with experimental data.

55 Milani et al. [24] performed a three-dimensional homogenized limit analysis to determine  
56 the ultimate lateral load of full masonry structures. Linearized homogenized surfaces  
57 for masonry in six dimensions [9, 23] were obtained and implemented in a finite element code.  
58 Comparisons between the predicted results from the 3D homogenized limit analysis and experimental  
59 data show an error of approximately 12%. Milani et al. [26] also used a 3D homogenized  
60 limit analysis for full masonry buildings reinforced by FRP. The error between the predicted  
61 results and experimental data for a two-story masonry building is 4.6% in absence of FRP  
62 and 9.4% in presence of FRP. Milani [20, 21] applied the 3D homogenized limit analysis to  
63 determine the limit load of a wall under in-plane and out-plane loading.

64 A simple equilibrium model was used to estimate the ultimate capacity of masonry shear  
65 walls. The model was based on strut-and-tie schemes representing the combination of the  
66 compression or tension stress fields at the ultimate condition. Comparisons between the performance  
67 of the model and experimental results for dry-joint and mortar-joint masonry show  
68 good agreement. [32]

69 A finite element analysis was conducted for a single-story, one-room masonry building, with  
70 different aspect ratios and with different positions of wall openings, subjected to a seismic force  
71 with varying direction [36]. The response spectrum method was employed for the analysis.  
72 The predicted results show that the critical direction of seismic force for the development of  
73 maximum stresses in the walls of a room occurs when the opening is along the short wall of  
74 the room. It was also observed that the maximum principle tensile stress occurred in the short  
75 wall, and the maximum shear stress occurred in the long wall.

76 The analysis of unreinforced masonry buildings employed a two-step approach [22]. In  
77 step 1, the ultimate bending moment – shear force strength domains of the masonry spandrels  
78 were derived by means of a heterogeneous upper-bound finite element limit analysis, and the  
79 results were stored in a database. In step 2, an equivalent frame model of the masonry wall  
80 was assembled. In the frame model, the spandrels were modeled as elastic Timoshenko beams.  
81 At each analysis step, a check was performed to determine whether the internal forces of these  
82 coupling beams were smaller than the failure loads stored in the database created in step 1.  
83 The shear force and bending moment capacity of the piers were simply estimated according  
84 to the Italian Design code. The proposed analysis approach was appeared capable of deriving  
85 the pushover curve of unreinforced masonry walls [22].

86 A constitutive model was developed on the basis of homogenized anisotropic elasto-plasticity.  
87 The effect of anisotropy was introduced by a fictitious isotropic stress and strain space. The  
88 advantage of this model is that the classical theory of plasticity can be used to model nonlinear  
89 behavior in the isotropic spaces [17].

90 A rigid-body numerical model was used to identify the minimum height-to-thickness ratio  
91 that would cause the wall to collapse when subjected to different out-of-plane ground motions

[35]. The spectral accelerations of the ground motions were selected to be 0.24 g, 0.3 g, 0.37 g and 0.44 g. The model was calibrated using the results of full-scale shake table tests of a wall with a height to thickness ratio of 12 [19]. The results of the analysis showed that when a wall is subjected to a spectral acceleration of 0.44 g, the probability of collapse for height-to-thickness ratios less than 10 is less than 1%. The ratios for spectral accelerations of 0.24 g and 0.3 g are 18 and 15, respectively [35]. Therefore, walls with the conditions described above will stabilize when subjected to out-of-plane ground motions, and the in-plane strength of the wall will be important in resisting lateral forces.

Akhaveissy [1] presented a new close form solution to determine the shear strength of unreinforced masonry walls. Predicted results show less error percentage than ATC and FEMA-307 [12]. The new explicit formula is based on results of proposed interface model by Akhaveissy [1]. Consequently, the proposed closed form solution can be used satisfactorily to analyze unreinforced masonry structures.

The research results discussed above that are related to macro-modeling processes show considerable differences between different methods of macro-modeling in comparison with test data [31]. Therefore, in this investigation, the closed-form solution by Akhaveissy [1] is extended to allow implementation in a macro-element approach using two-noded linear elements in a finite element framework. The analysis time is decreased in comparison with analyses performed using the micro-element approach and the finite element method, which use solid elements and shell elements. Moreover, the accuracy of the analysis is increased because the formulation is based on the micro-element approach.

## 2 THE CLOSE FORM SOLUTION

The closed form solution to determine the resistance lateral force of unreinforced masonry wall is based on the effective width of the wall in compression [1]. The effective width of unreinforced masonry wall is in terms of the height-to-width ratio of the wall. The width of the compressive diagonal is proposed as a coefficient of the length of the diagonal [1]. This coefficient is shown by  $F_w$ . Fig. 1 shows variations of the coefficient versus different height/width ratio of the wall [1].

Hence, the resistance lateral force is based on compressive axial force of the effective width, Fig. 2.

According to Fig. 2, the resistance lateral force is as follows [1]:

$$\begin{aligned} P &= P_d * \text{COS}(\theta) \\ P_d &= F_w L_d t \sigma_d ; \sigma_d = 2 \tau_u \\ \tau_u &= C + \sigma_0 \tan(\phi) \end{aligned} \quad (1)$$

where,  $C$  and  $\phi$  are the cohesive strength and the friction angle, respectively. In Eq. (1),  $\sigma_0$  is the initial applied pressure on the top of the wall. The lateral strength of different unreinforced masonry walls analyzed by Eq. (1) and Fig. 1 [1]. Predicted results compared with test data and FEMA guideline [12]. The comparisons show good correlation between predicted results

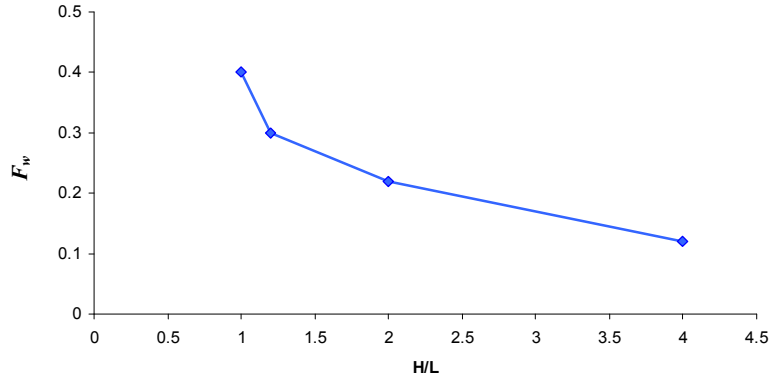


Figure 1 The coefficient of compressive diagonal versus high to width ratio of wall [1]

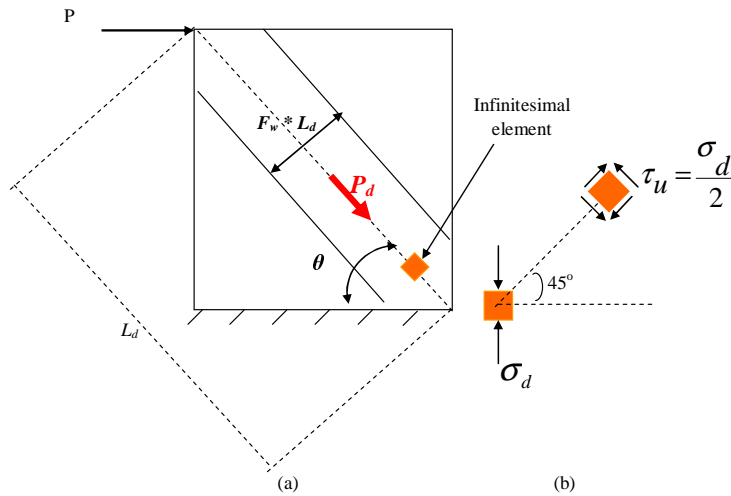


Figure 2 a) compressive effective width of the wall and b) principal stress on infinitesimal element [1]

127 of Eq. (1) and test data. The closed form solution, Eq. (1), predicts the ultimate lateral load  
 128 of unreinforced masonry walls less error percentage than ATC and FEMA-307 [12]. Hence, Eq.  
 129 (1) is used to determine the shear strength of piers and spandrels in an unreinforced masonry  
 130 frame. Therefore, the internal forces of two-noded linear elements in finite element method  
 131 are compared with predicted strength by Eq. (1).

### 132 3 MACRO-ELEMENT MODEL

133 In this study, different unreinforced masonry (URM) structures are analyzed based on Eq.  
 134 (1). A macro-element method is used for the analysis of URM structures based on two-noded  
 135 linear elements. Then, a force–displacement relationship and an algorithm are presented to  
 136 analyze URM structures using macro-elements. The stiffness matrix of the element included  
 137 both bending and axial stiffness matrices. Fig. 3 shows the shape functions of the elements

138 for both parts.

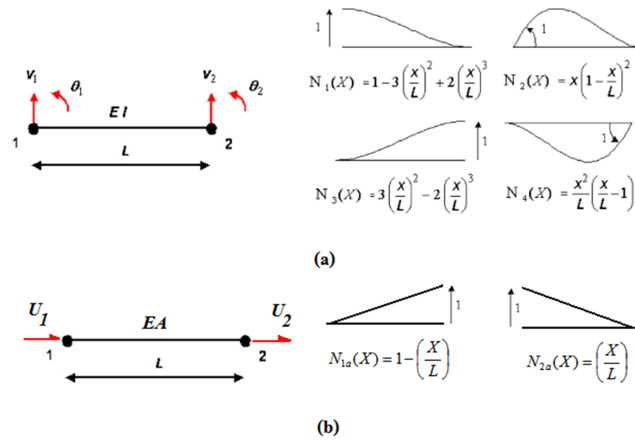


Figure 3 Bernoulli beam element and shape function for the a) bending effect and b) axial effect

139 The initial stiffness method is used in the analysis. Therefore, assuming a linear elastic ma-  
 140 terial with a stress-strain relationship of  $\{\sigma\} = [E] \{\varepsilon\}$  and a strain-displacement relationship  
 141 of  $\{\varepsilon\} = [B] \{d\}$ , the element bending stiffness matrix can be determined from the following  
 142 relationship:

$$K_b = \int_0^L [B]^T [EI] [B] dx; [B] = \frac{d^2}{dx^2} [ N_1 \quad N_2 \quad N_3 \quad N_4 ] \quad (2)$$

143 After integration using the element shape functions, the elemental bending stiffness  $K_b$  is found  
 144 to be the following:

$$K_b = \frac{EI}{L^3} \begin{bmatrix} 12 & 6L & -12 & 6L \\ 6L & 4L^2 & -6L & 2L^2 \\ -12 & -6L & 12 & -6L \\ 6L & 2L^2 & -6L & 4L^2 \end{bmatrix} = \begin{bmatrix} K_{b11} & K_{b12} \\ K_{b21} & K_{b22} \end{bmatrix} \quad (3)$$

145 The element axial stiffness matrix can be expressed using the following relationship:

$$K_a = \int_0^L [B]^T [EA] [B] dx; [B] = \frac{d}{dx} [ N_{1a} \quad N_{2a} ] \quad (4)$$

146 After integration using the element shape functions, the elemental axial stiffness  $K_a$  is found  
 147 to be the following:

$$K_a = \frac{EA}{L} \begin{bmatrix} 1 & -1 \\ -1 & 1 \end{bmatrix} = \begin{bmatrix} K_{a11} & K_{a12} \\ K_{a21} & K_{a22} \end{bmatrix} \quad (5)$$

148 The elemental stiffness for the local axis is obtained by combining Eq. (3) and Eq. (5) to  
 149 arrive at the following equation:

$$K = \begin{bmatrix} K_{a11} & 0 & K_{a12} & 0 \\ 0 & K_{b11} & 0 & K_{b12} \\ K_{a21} & 0 & K_{a22} & 0 \\ 0 & K_{b21} & 0 & K_{b22} \end{bmatrix} \quad (6)$$

150 The stiffness matrix of elements in the global axis is determined using rotation forces from the  
 151 local axis to the global axis and is expressed as the following:

$$K_G = [R]^T [K] [R]$$

$$[R] = \begin{bmatrix} R_1 & 0 \\ 0 & R_2 \end{bmatrix}; \quad R_1 = R_2 = \begin{bmatrix} \cos \theta & \sin \theta & 0 \\ -\sin \theta & \cos \theta & 0 \\ 0 & 0 & 1 \end{bmatrix} \quad (7)$$

152 Here,  $\theta$  is the angle between the axis of the element and the horizontal axis in the anticlockwise  
 153 direction.

154 The solution to the equilibrium equation system yields the joint displacements and internal  
 155 forces in the local coordinate system. The internal forces cause damage to the masonry wall.  
 156 Therefore, the internal forces should be compared with the nonlinear behavior of masonry  
 157 walls. This comparison is discussed in the next section.

### 158 3.1 Deformation capacity and stiffness evaluation

159 The response of brick masonry walls is strongly nonlinear, even at low load levels, because of  
 160 the low tensile strength of the bed and head joints. As the damage due to cracking increases,  
 161 masonry walls show both strength and stiffness degradation. A definition of the elastic stiffness  
 162 of a wall subjected to in-plane shear must be related to a reference stress or deformation. A  
 163 common approach followed for design and assessment purposes is to idealize the cyclic envelope  
 164 with a bilinear curve. In Fig. 4, possible definitions of the parameters of the bilinear curve are  
 165 presented. The value of  $V_u$  is determined by Eq. (1). In other words,  $V_u$  is equal to parameter  
 166 P in Eq. (1). The initial elastic stiffness of a masonry wall is evaluated using Eq. (7). Fig.  
 167 4 also shows the acceptance criteria for the primary elements according to FEMA 356 [13].  
 168 Accordingly, the value of drift for the immediate occupancy criterion, the life safety level and  
 169 the collapse prevention level are 0.1%, 0.3% and 0.4%, respectively. The acceptance criteria  
 170 provided by FEMA356 [13] are also valid when evaluating damage to unreinforced masonry  
 171 structures. However, the ultimate shear force for piers and spandrels is determined by Eq. (1).

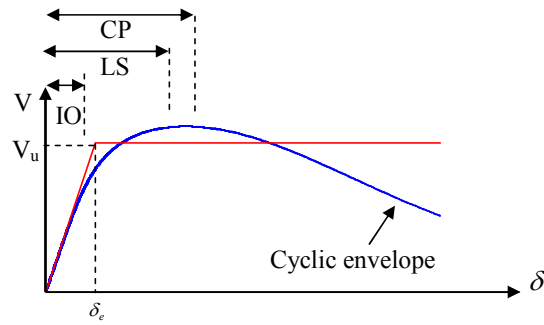


Figure 4 Definition of an equivalent bilinear envelope

### 172 3.2 Proposed algorithm

173 An algorithm is proposed for nonlinear analysis of URM structures based on the macro-element  
 174 method and a force–displacement relationship. Table 1 shows the solution process.

Table 1 Proposed algorithm

1	definition of geometry, material and loading, including the dead and live load and lateral load
2	determination of the elastic stiffness matrix for each element based on Eq. (7) and the stiffness matrix of the total structure
3	determination of the dead and live load vectors for the URM structure
4	solution of the system of equations for step 3
5	establishment of the incremental load vector for the lateral load
6	solution of the system of equations based on step 2
7	determination of the internal force vector in the local axes for each element
8	evaluation of the internal forces for nonlinear behavior (see Table 2)
9	determination of the residual force vector for the URM structure
10	evaluation of the convergence criterion based on the L2 norm of the residual force
11	if the value of the L2 norm is less than the value of the error provided by the user, then go to step 5 and evaluate the last incremental lateral force vector, otherwise go to step 6 and solve the system of equations for the residual force vector

175 A program in the FORTRAN language is prepared from the algorithm presented in Tables 1  
 176 and 2. Different unreinforced masonry structures are analyzed using the program. Predictions  
 177 from the program are compared with laboratory data and numerical analyses based on different  
 178 solution procedures.



Table 2 Evaluation of URM wall resistance

1	Determine $F_w$ using Fig. 1. $F_w$ for H/L greater than 4 is determined from a linear equation between H/L=2 and H/L=4 However, if $F_w \leq 0 \Rightarrow F_w = 0$
2	determination of the axial stress, $\sigma$ , based on the axial force, P, in the local axes. The axial stress is assumed negative for tensile stress and positive for compressive stress.
3	<p>if <math>\sigma \leq</math> then</p> <p>if <math>\sigma &lt; -f_t</math> then</p> <p>Value of all internal forces is assumed equal to zero</p> <p>else</p> <p><math>\tau_u = C + \sigma \tan(\varphi)</math></p> <p>if <math>\tau_u &lt; 0</math> then <math>\tau_u = 0</math></p> <p><math>\sigma_d = 2 * \tau_u</math></p> <p><math>V_u = F_w L_d t \sigma_d</math></p> <p>if <math>V_u &gt; V_{int}</math> then the behavior of the wall is elastic and internal shear force, <math>V_{int}</math>, is not changed</p> <p>if <math>V_u \leq V_{int}</math> then</p> <p><math>f = \frac{V_u}{V_{int}}</math></p> <p><math>V_{int} = V_u * \frac{V_{int}}{ V_{int} }</math></p> <p><math>M_{int} = M_{int} * f</math></p> <p>endif</p> <p>else</p> <p>if <math>\sigma &gt; f_c</math> then</p> <p><math>\sigma = f_c</math></p> <p><math>P = \sigma * A * \frac{P}{ P }</math></p> <p>endif</p> <p><math>\tau_u = C + \sigma \tan(\varphi)</math></p> <p><math>\sigma_d = 2 * \tau_u</math></p> <p><math>V_u = F_w L_d t \sigma_d</math></p> <p>if <math>V_u &gt; V_{int}</math> then the behavior of the wall is elastic and internal shear force, <math>V_{int}</math>, is not changed</p> <p>if <math>V_u \leq V_{int}</math> then</p> <p><math>f = \frac{V_u}{V_{int}}</math></p> <p><math>V_{int} = V_u * \frac{V_{int}}{ V_{int} }</math></p> <p><math>M_{int} = M_{int} * f</math></p> <p>endif</p> <p>end, if</p>

## 179 4 APPLICATIONS

### 180 4.1 A single-story unreinforced masonry building

181 A full-scale single-story unreinforced masonry building tested in the laboratory by Paquette  
 182 and Bruneau [27–29] was chosen to validate the model. Fig. 5 shows the west wall of the  
 183 tested model. The parapet of the west wall and the east wall was 254 mm tall[27].

184 The compressive strengths of the brick and mortar were 109 and 9.24 MPa, respectively,  
 185 and the compressive and tensile strengths of the masonry were 22.2 and 0.18 MPa, respectively  
 186 [27]. These strengths were used for the numerical analysis of the west wall by the DSC/HISS-  
 187 CT model [2]. The thickness of the wall was 190 mm. The gravity load,  $2.4 \text{ kN/m}^2$ , was  
 188 applied on the diaphragm, whose dimensions were 4091 mm \* 5610 mm. Ten wood joists were

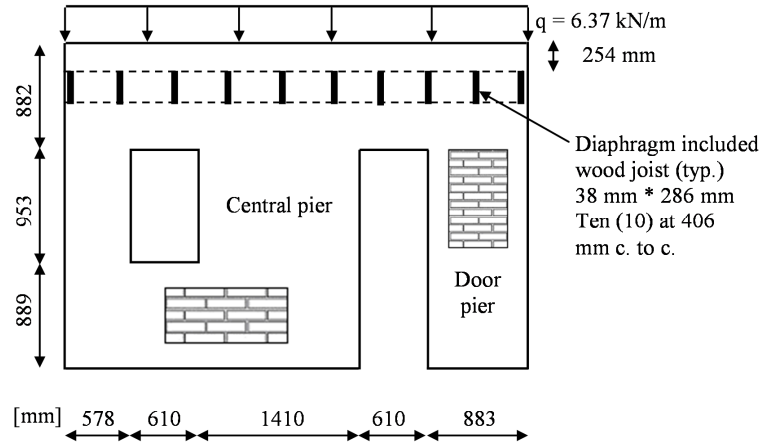


Figure 5 Dimensions of the west wall in mm [27]

189 applied to the diaphragm to transmit the gravity load to the west and east walls. The net span  
 190 of the wood joist was 5310 mm [27]. Therefore, the gravity load on each wall was 6.37 kN/m.  
 191 The mesh for the west wall contained 720 eight-node isoparametric elements and 2527 nodes;  
 192 the number of degrees of freedom was 4926 [2]. The west wall was also analyzed to determine  
 193 the ultimate base shear force by Akhveissy [1]. The cohesion strength and the friction angle  
 194 for the analysis were equal to 0.078 MPa and 31.9 degree, respectively [1]. The wall is chosen  
 195 to show capability of the proposed algorithm in Table 1 and 2. Fig. 6 shows the equivalent  
 196 frame model for the analysis. The number of degrees of freedom in present work is 9 and the  
 197 error for the evaluation of convergences is considered to be 1e-10.

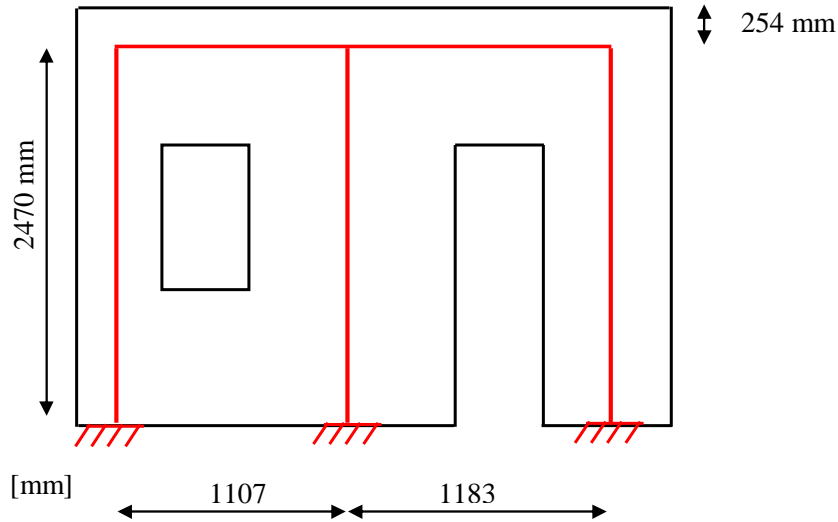


Figure 6 Equivalent frame model for the west wall

198 Test data and predicted results in present work are compared in Fig. 7. Predicted pushover

199 curve shows good correlation with test data. Fig. 7(b) shows comparison of the results for  
 200 displacement at top of wall between 0 to 3 mm. The predicted base shear force by DSC/HISS-  
 201 CT model and Equivalent frame model are 22.7 kN and 22.5 kN, respectively. Value of the  
 202 base shear force is observed 22.8 kN [27]. Hence, the ultimate lateral load is estimated with  
 203 proper accuracy by both models.

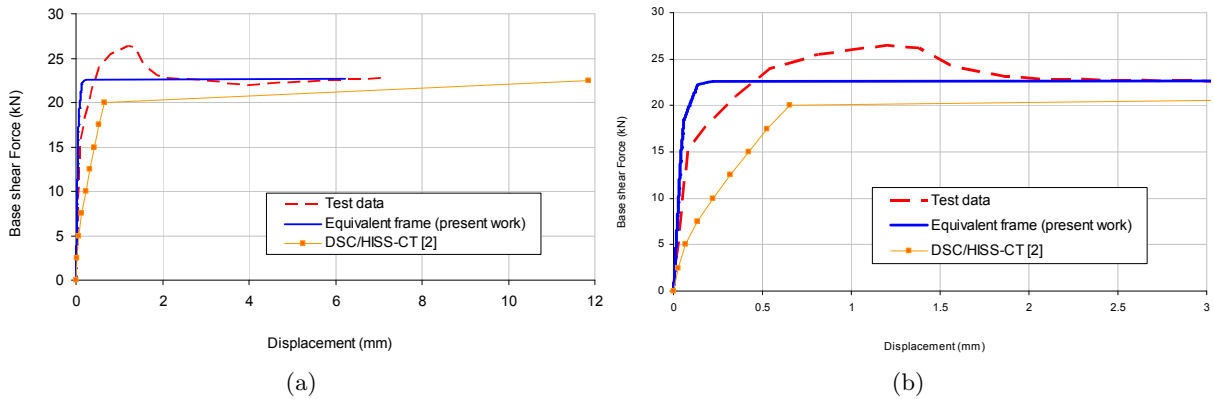


Figure 7 a) Comparison of predicted results with test data for the west wall and b) detailed illustration of the results

204 The initial slope of the equivalent frame in present work correlates with test data, Fig.  
 205 7(b). However, predicted results by DSC/HISS-CT [2] shows less accuracy than the equivalent  
 206 frame.

## 207 4.2 A two-bay, two-story building

208 A full-scale, two-story unreinforced masonry building tested at Pavia University was chosen  
 209 for model validation [18]. This structure has been extensively studied in the literature [4, 8].  
 210 The building, with a 6\*4.4 m floor plan and 6.4 m in height, contains an almost independent  
 211 shear wall that is in-plane loaded. The wall considered here (named the “door wall”) is 250  
 212 mm thick and has two doors on the first story and two windows on second story, as shown  
 213 in Fig. 8. The door wall includes two exterior piers and one interior pier. The exterior pier  
 214 width and axial loads on the bottom and top levels are equal to 1.15 m, 56 kN and 26.9 kN,  
 215 respectively. The interior pier width and axial loads on the bottom and top levels are equal to  
 216 1.82 m, 133 kN and 64.5 kN, respectively.

217 The properties of the structure used in the model are summarized below[4]:

218 The maximum compressive strength of a masonry prism,  $f_m$ , is equal to 7.9 MPa. The joint  
 219 tensile strength and the joint cohesion are 0.07 MPa and 0.14 MPa, respectively. The joint  
 220 coefficient of friction is 0.55. The shear modulus is equal to the effective value,  $G_{eff} = 90f_m$ .  
 221 Fig. 9 shows comparisons between the present work and experimental data and numerical  
 222 analyses [8]. Calderini et al. [8] used the finite element method (FEM) to analyze the two-  
 223 story unreinforced masonry building tested at Pavia University. The model included 2696  
 224 nodes and 5128 triangular shell elements. The predicted results were compared with results

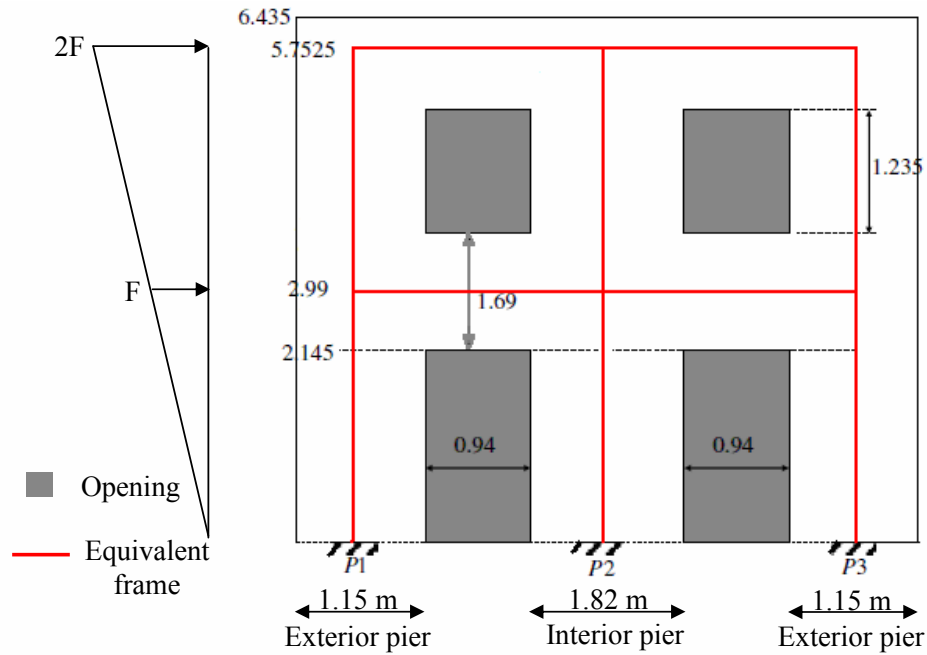


Figure 8 Door wall of the full-scale, two-story unreinforced masonry building tested at Pavia University

225 obtained using the equivalent frame model and the Tremuri software [8]. The equivalent frame  
 226 included 9 nodes, and 3 nodes were fully constrained at the base. The reduce stiffness and full  
 227 stiffness were used to analyze the building with the equivalent frame.

228 Fig. 9 shows that the equivalent frame–reduce stiffness model predicted that the stiffness  
 229 of the building would be lower than the real stiffness. The value of the ultimate base shear  
 230 force from the Tremuri software was estimated to be 167 kN whereas the experimental value  
 231 was determined to be 147 kN. The value of ultimate base shear force from the present work  
 232 and from Belmouden and Lestuzzi [4] was predicted to be 147 kN and 137.6 kN, respectively.  
 233 The finite element method estimate of the force was 157 kN. Fig. 9 shows a better agreement  
 234 between the test data and the present work than with other models. To consider the damage  
 235 to the structure, the acceptance criteria are evaluated in Fig. 10. The equivalent frame in the  
 236 present work included 9 nodes, and 3 nodes were fully constrained at the base. The applied  
 237 base shear force equal to the lateral load is 150 kN, which is prepared in 400 steps. The  
 238 tolerance for both the displacement convergence criterion and the force convergence criterion  
 239 is  $1 \cdot 10^{-10}$ . The analysis of the URM structure for step 389 converged after 1434 iterations  
 240 whereas the analysis is not converged after 45,000 iterations for step 390. The total time  
 241 of the calculation is 4.78 sec. The value of the displacement at the roof for step 389, after  
 242 1434 iterations, is 14.10 mm; however, the value of the displacement for step 390 after 45,000  
 243 iterations is 179.23 mm.

244 Crack patterns from the experimental test of the URM building at the failure state (a top

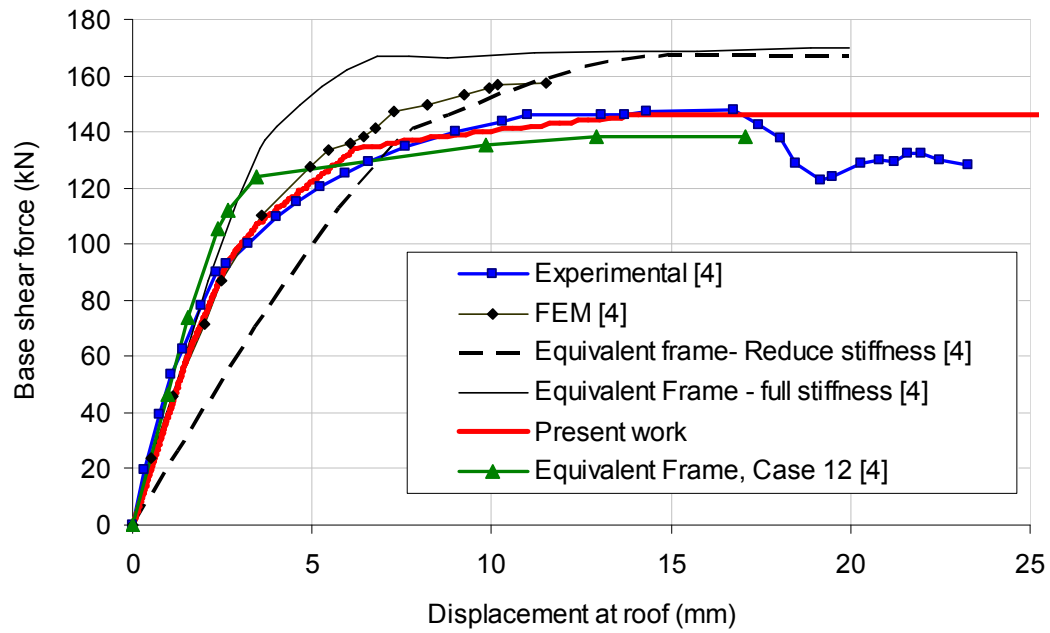


Figure 9 Comparison of the predicted results with experimental data for the two-story unreinforced masonry building tested at Pavia University

245 displacement equal to 24 mm) show damage to the piers for the second story and the first  
 246 story as well as damage to the spandrels at the first floor. The predicted failure of the piers  
 247 correlates with the observed data while the damage to the spandrels is not seen in the present  
 248 work. This difference is due to the dissipation of energy by the piers. Hence, the spandrel  
 249 beams behave as elastic beams.

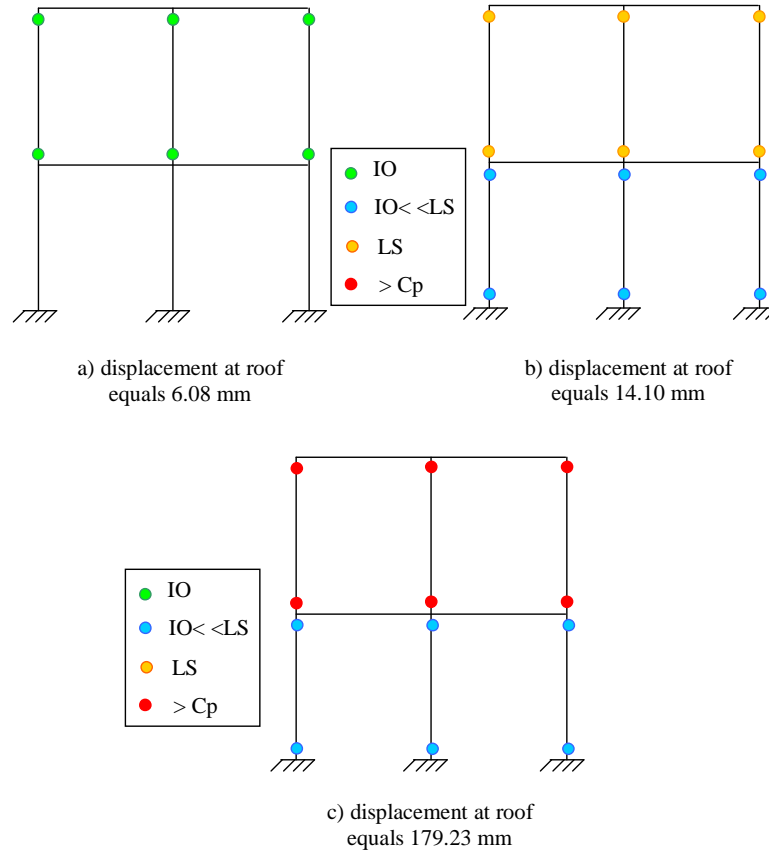


Figure 10 Damage levels for the URM structure from the present work for a) displacement at the roof equals 6.08 mm, b) displacement at the roof equals 14.10 mm and c) displacement at the roof equals 179.23 mm

250 **4.3 A seven-bay, two-story building**

251 In the present work, two different unreinforced masonry building are analyzed. A one-bay  
 252 frame and a seven-bay frame with two stories are analyzed to evaluate the capability of the  
 253 model. The structures are shown in Fig. 11. These unreinforced masonry frames were analyzed  
 254 by Salonikios et al. [34]. Details of the structures are explained as follows. In addition to the  
 255 self-weight of the masonry, extra masses are considered at the floor levels. For the one-bay  
 256 frame, a uniformly distributed mass of 6 tons/m was assumed for the first floor, and 4 tons/m  
 257 was assumed for the second floor [11, 34]. The corresponding values for the seven-bay frame  
 258 were assumed to be 3 and 2 tons/m, respectively [34]. The mechanical characteristics of the  
 259 masonry material were as follows: the thickness of the walls was equal to 0.6 m, the volumetric  
 260 mass was  $\rho = 2t/m^3$ , the Young's modulus was  $E=1650$  MPa, the Poisson ratio was  $\nu = 0.2$ ,  
 261 the tensile strength was  $f_t=0.1$  MPa, and the compressive strength was  $f_c=3.0$  MPa. The joint  
 262 cohesion and the joint friction angle were 0.09 MPa and  $30^\circ$ , respectively [34].

263 Fig. 12. shows equivalent frames for the one-bay and seven-bay two-story masonry build-

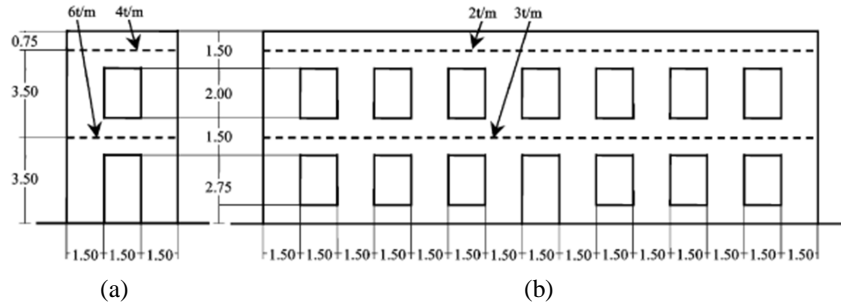


Figure 11 a) One-bay and b) seven-bay two-story masonry buildings

ings with the lateral load pattern.

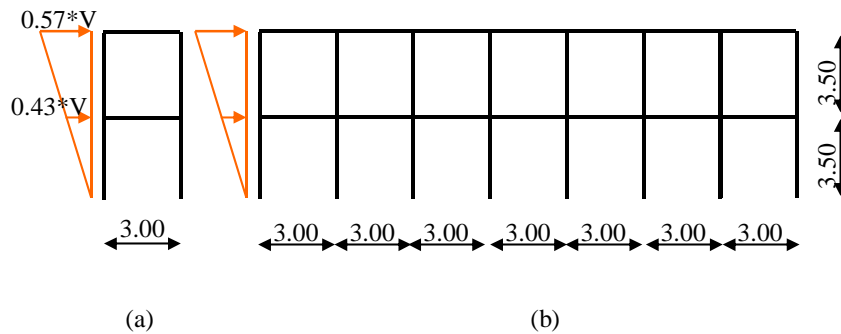
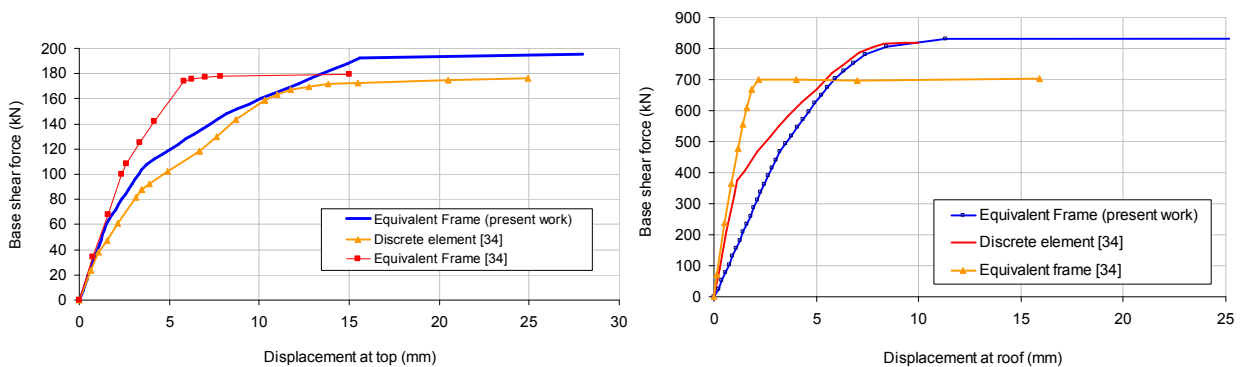


Figure 12 Equivalent frame and lateral load pattern for a) one-bay and b) seven-bay two-story buildings

264  
 265 In Fig. 12,  $V$  is the value of the base shear force on the masonry buildings at the failure  
 266 mode. Each node in Fig. 12 included two transitive degrees of freedom and one rotational  
 267 degree of freedom. Hence, the numbers of degrees of freedom for the one-bay building and  
 268 the seven-bay building are 12 and 48, respectively. The total number of elements for the  
 269 masonry buildings in Fig. 12(a) and (b) are 6 and 30, respectively. Salonikios et al.[34]  
 270 used the equivalent frame and discrete element methods to analyze the one-bay and seven-bay  
 271 buildings. The presented relations in the FEMA guidelines were used in the equivalent frame  
 272 method. The number of elements and degrees of freedom for both masonry buildings were the  
 273 same as in the present work. The number of nodes, degrees of freedom and elements were 518,  
 274 1008 and 444, respectively, for the one-bay, two-story building in the discrete element method.  
 275 Salonikios et al. [34] used element dimensions of  $0.2 \times 0.1$  for the one-bay frame and  $0.5 \times 0.25$   
 276 for the seven-bay frame. Hence, the number of nodes, degrees of freedom and elements were  
 277 2402, 4632 and 2100, respectively, for the seven-bay frame in the discrete element method.  
 278 Consequently, the solution time is less with the equivalent frame method. The solution time in

279 the present work using the equivalent frame model is 0.3 and 0.7 sec for the one-bay and seven-  
 280 bay frames, respectively. The tolerance for both the displacement and the force convergence  
 281 criteria is  $1e-5$  for the one-bay frame and  $1e-12$  for the seven-bay frame. The total number of  
 282 converged steps is 49 steps out of 50 steps for the one-bay frame and 33 steps out of 50 steps  
 283 for the seven-bay frame. The analysis of the one bay structure for step 49 converged after 161  
 284 iterations whereas the analysis is not converged after 400 iterations for step 50. The analysis  
 285 of the seven bays structure for step 33 converged after 1396 iterations. A comparison of the  
 286 pushover curve from the present work and that predicted by Salonikios et al. [34] is shown in  
 287 Fig. 13 for both buildings. The value of the displacement at the roof of one bay frame for step  
 288 49, after 161 iterations, is 15.163 mm; however, the value of the displacement for step 50 after  
 289 400 iterations is 27.994 mm. The value of the displacement at the roof of seven bays frame for  
 290 step 33 is 11.33 mm; however, the value of the displacement for step 34 after 1400 iterations  
 291 is 141.699 mm.



(a) the pushover curve for the one-bay, two-story masonry building (b) the pushover curve for the seven-bay, two-story masonry building

Figure 13 Comparisons of the pushover curves from the equivalent frame model and the discrete element method

292 The values of the base shear force for the one-bay and seven-bay masonry structures pre-  
 293 dicted in the present work are 190 kN and 794 kN, respectively. These values are 177 kN and  
 294 819 kN when using the discrete element method and 180 kN and 705 kN using the equivalent  
 295 frame method as presented in the study by Salonikios et al.[34] . Accordingly, the predicted  
 296 results in present work correlate well with the results of the discrete element method. The pre-  
 297 dicted pushover curve from the equivalent frame model by Salonikios et al. [34] shows a nearly  
 298 elastic-perfectly plastic behavior; however, the predicted pushover curve from the equivalent  
 299 frame model in present work shows a flexible behavior that is similar to the curve from the  
 300 discrete element method with the numerous number of degrees of freedom. Fig. 14 shows the  
 301 plastic hinges for the masonry structures in accordance with points A and B in Fig. 13.



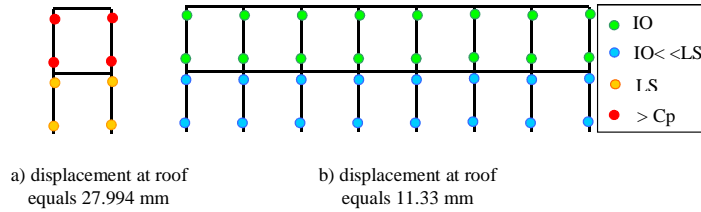


Figure 14 The plastic hinges for the one-bay and seven-bay two-story masonry buildings from the present analysis for points A and B in Fig. 13

302 **4.4 Application to an old masonry building**

303 An inner wall of a five-story building located in Via Martoglio (Catania, Italy) is analyzed  
 304 using Eq. (1) and the presented algorithm, as shown in Tables 1 and 2. The full geometric  
 305 characterization of the panel in the present analysis is shown in Fig. 15. The building was  
 306 analyzed by Brencich et al. [6]. The four-node element with 2\*2 Gauss points was used in the  
 307 analysis. The model included 17,000 degrees of freedom. This building was also analyzed by  
 308 Milani et al. [25]. The lower bound analysis utilized 1000 triangular elements. The thickness  
 309 of last story is 160 mm while the thickness of the other stories is 300 mm. Numerical values  
 310 used in the present analysis, as shown in Table 3, are adopted from Brencich et al.[6].

Table 3 Mechanical properties of the masonry unit and joints [6]

c (MPa)	$f_t$ (MPa)	$f_m$ (MPa)	$\phi$
0.15	0.1	3.00	26.56

311 Here,  $f_t$  is the tensile strength,  $f_m$  is the compressive strength, c is the cohesion and  $\phi$  is  
 312 the friction angle.

313 The equivalent static forces at the levels of stories were calculated in Brencich et al.[6] , as  
 314 shown in Table 4.

Table 4 Equivalent static forces for the five-story masonry building [6]

Level	Unit weight of masonry $\gamma = 17 \text{ kN/m}^3$					
	0	1	2	3	4	5
Thickness of wall (mm)	300	300	300	300	300	160
Masonry weight (kN)	264.70	480.55	486.70	486.70	373.15	129.80
Applied load on stories (kN)	305.05	305.05	372.90	372.90	372.90	53.70
Total weight (kN)	569.75	785.60	859.60	859.60	746.05	183.50
$h_i$ (m)	0.64	4.52	8.22	11.92	15.62	19.12
$\gamma_i = h_i \sum_{j=1}^n W_j / \sum_{j=1}^n W_j h_j$	0.0704	0.4974	0.9045	1.2786	1.7187	2.1038
$F_h = W * C * R * \varepsilon * \beta * I * \gamma$ $I = 1.$ $\varepsilon = 1.$ $R = 1.$ $\beta = \beta_1 * \beta_2 = 4.$ $S = 12 \Rightarrow C = 0.1$						
Equivalent static force $F_h$ (kN):	16.05	156.30	311.00	439.65	512.90	154.40

315 The equivalent frame model and the seismic loads on the old five-story masonry building  
 316 are shown in Fig. 16.

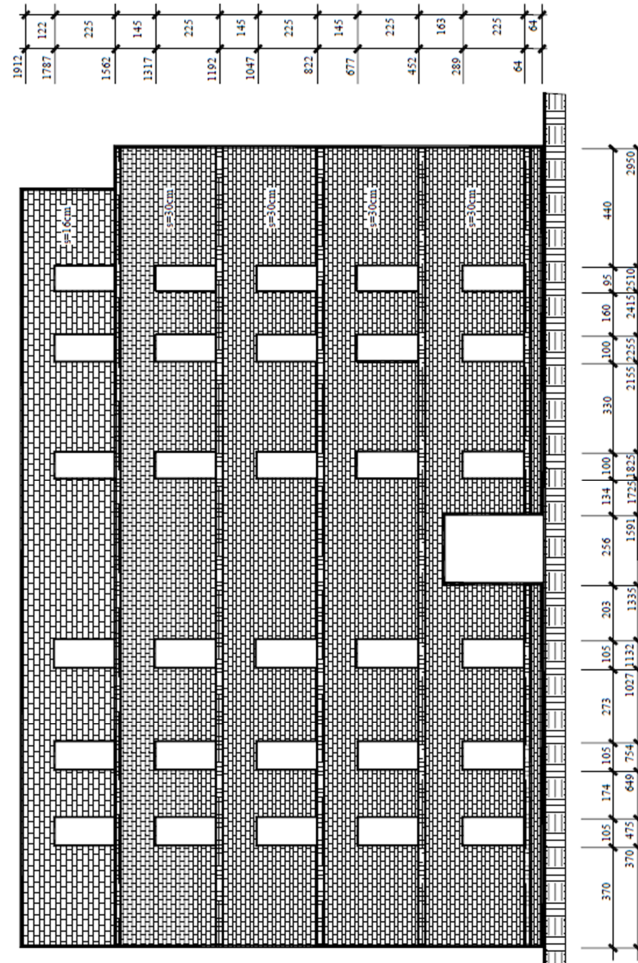


Figure 15 Geometric diagram of the inner wall of a five-story building [6]

317 The equivalent frame model in present work included 75 linear elements and 120 degrees of  
 318 freedom (DOFS). The tolerance for both the displacement convergence criterion and the force  
 319 convergence criterion is  $1 \cdot 10^{-12}$ . The model is analyzed using the algorithm in Tables 1 and  
 320 2. The total time of the calculation is 144 sec. The predicted pushover curve from the present  
 321 analysis is compared in Fig. 17 with a predicted curve using the discrete element method with  
 322 17,000 DOFS.

323 Fig. 17 shows good agreement between the results of the equivalent frame model and the  
 324 discrete element method for the hardening branch. The value of the ultimate base shear force  
 325 is 1430 kN using the equivalent frame model and 1258 kN using the discrete element method.  
 326 The difference between the ultimate base shear forces for both models is less than 13.7%. Fig.  
 327 18 shows the distribution of the plastic hinges in accordance with point A in Fig. 17. When  
 328 the displacement of the roof equals 49.963 mm, point A in Fig. 17, the performance level of

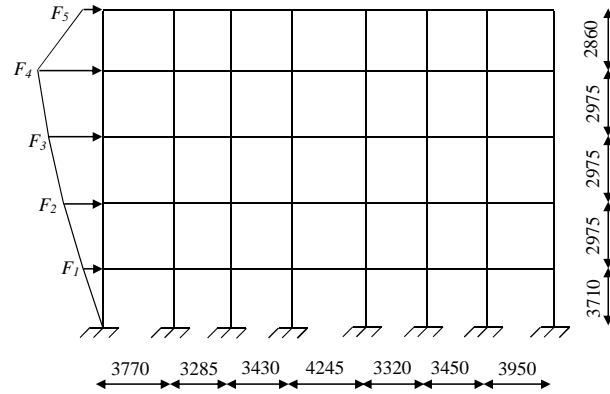


Figure 16 Equivalent frame model and seismic loads

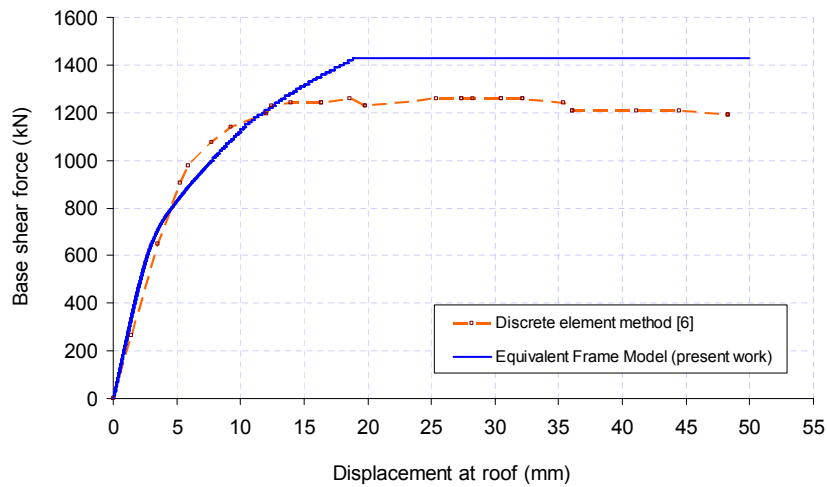


Figure 17 Comparison of the results from the present work with 120 DOFS and the discrete element method with 17,000 DOFS

329 the masonry piers in the first floor is between the immediate occupancy level and the life safety  
 330 level, and the value of the drift for the piers is 0.002. The performance levels of the masonry  
 331 piers for other stories indicate previous collapse, and the values of the drift for the piers are  
 332 variable and between 0.0033 and 0.0037.

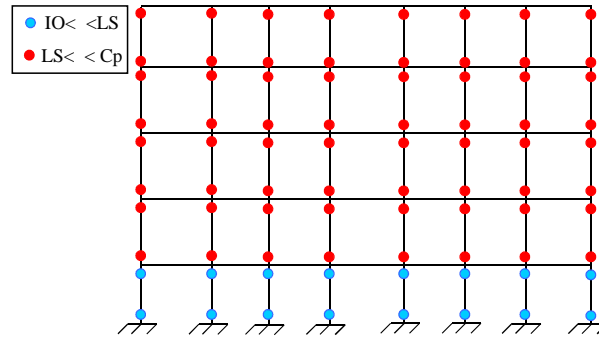


Figure 18 Distribution of plastic hinges for the old five-story unreinforced masonry building when the displacement of the roof equals 49.963 mm, point A in Fig. 17

## 333 5 CONCLUSION

334 The paper presents nonlinear analysis of unreinforced masonry buildings. The analysis is used  
 335 finite element procedure and a close form solution proposed by Akhveissy [1]. The close  
 336 form solution was determined based on a new interface model for modeling the mechanical  
 337 response of mortar joints in masonry walls. The interface laws were formulated in the frame-  
 338 work of elasto-plasticity for non-standard materials with softening, which occurs in mortar  
 339 joints because of applied shear and tensile stresses. The Von Mises criterion was used to  
 340 simulate the behavior of the units. The interface laws for contact elements were formulated  
 341 to simulate the softening behavior of mortar joints under tensile stress. A normal linear cap  
 342 model was also used to limit compressive stress. The capabilities of the interface model and  
 343 the effectiveness of the computational procedure were investigated using numerical examples  
 344 that simulate the response of a masonry wall tested under shear in the presence of an initial  
 345 pre-compression load. The computer predictions correlated very well with the test data. The  
 346 closed-form solution was better than ATC and FEMA 273 at predicting the ultimate lateral  
 347 load of unreinforced masonry walls. Hence in the present work, the new closed-form solution  
 348 is implemented in a finite element method using two-noded linear elements. An algorithm  
 349 is presented for this purpose. Different masonry structures, including low- and high-rise ma-  
 350 sonry buildings, are analyzed using the new closed-form solution and the presented algorithm.  
 351 A comparison of results from the present work with experimental data and previous works  
 352 show proper accuracy from the present work. Consequently, the proposed closed-form solution  
 353 and the presented algorithm can be used to satisfactorily analyze masonry structures similar  
 354 to those considered in this work. The finite element method with two-noded linear element  
 355 and presented algorithm show proper accuracy for analysis of low- and high-rise unreinforced  
 356 masonry buildings. Hence, the proposed model can be used to predict the base shear force  
 357 of unreinforced masonry structures under earthquake acceleration in nonlinear finite element  
 358 analyses. Therefore, practicing engineers can determine the behavior of an URM building and  
 359 its performance level with proper accuracy under seismic excitation using concepts described  
 360 in the present work.

## References

- 361 [1] A.H. Akhveissy. Lateral strength force of URM structures based on a constitutive model for interface element. *Latin*  
362 *American Journal of Solids and Structures*, 8:445–461, 2011.
- 364 [2] A.H. Akhveissy and C.S. Desai. Unreinforced masonry walls: Nonlinear finite element analysis with a unified  
365 constitutive model. *Archives of Computational Methods in Engineering*, 18:485–502, 2011.
- 366 [3] C. Alessandri and C.A. Brebbia. Strength of masonry walls under static horizontal loads: boundary element analysis  
367 and experimental tests. *Engineering Analysis*, 4(3):118–134, 1987.
- 368 [4] Y. Belmouden and P. Lestuzzi. An equivalent frame model for seismic analysis of masonry and reinforced concrete  
369 buildings. *Construction and Building Materials*, 23:40–53, 2009.
- 370 [5] A. Brencich, L. Gambarotta, and S. Lagomarsino. A macroelement approach to the three-dimensional seismic  
371 analysis of masonry buildings. In *11th European Conference on Earthquake Engineering*, Rotterdam, 1998. Balkema.  
372 ISBN 9054109823.
- 373 [6] A. Brencich, L. Gambarotta, and S. Lagomarsino. Analysis of a masonry building in via martoglio. pages 107–143,  
374 2000. Catania Project: Research on the seismic response of two masonry buildings, chapter 6, University of Genoa  
375 (in Italian), CNR Gruppo Nazionale per la Difesa dei Terremoti.
- 376 [7] M. Bruneau. State-of-the-art report on seismic performance of unreinforced masonry buildings. *Journal of Structural*  
377 *Engineering*, 120(1):230–251, 1994.
- 378 [8] C. Calderini, S. Cattari, and S. Lagomarsino. In plane seismic response of unreinforced masonry walls: comparison  
379 between detailed and equivalent frame models. In M. Papadrakakis, N.D. Lagaros, and M. Fragiadakis, editors, *COM-*  
380 *PDYN 2009, ECCOMAS Thematic Conference on Computational Methods in Structural Dynamics and Earthquake*  
381 *Engineering In*, pages 22–24, Rhodes, Greece, June 2009.
- 382 [9] A. Cecchi and G. Milani. A kinematic fe limit analysis model fot thick english bond masonry walls. *International*  
383 *Journal of Solids and Structures*, 45:1302–1331, 2008.
- 384 [10] K. Chaimoon and M.M. Attard. Experimentatl and numerical investigation of masonry under three-point bending  
385 (in-plane). *Engineering Structures*, 31:103–112, 2009.
- 386 [11] I.O. Demirel. *A nonlinear equivalent frame model for displacement based analysis of unreinforced brick masonry*  
387 *buildings*. Dissertation, Middle East Technical University, 2010.
- 388 [12] Federal Emergency Management Agency (FEMA-307), Washington (DC). *Evaluation of earthquake damaged concrete*  
389 *and masonry wall buildings*, 1999. Technical Resources Publication no. 307.
- 390 [13] Federal Emergency Management Agency (FEMA-356), Washington (DC). *NEHRP Guidelines for the seismic reha-*  
391 *ilitation of buildings*, 2000.
- 392 [14] A. Gabor, E. Ferrier, Jacquelin, and P. Hamelin. Analysis and modeling of the in-plane shear behavior of hollow  
393 brick masonry panels. *Construction and Building Materials*, 20:308–321, 2006.
- 394 [15] H.B. Kaushik, D.C. Rai, and S.K. Jain. Stress-strain characteristics of clay brick masonry under uniaxial compression.  
395 *Journal of Material in Civil Engineering ASCE*, 19(9):728–739, 2007.
- 396 [16] H.B. Kaushik, D.C. Rai, and S.K. Jain. Uniaxial compressive stress-strain model for clay brick masonry. *Current*  
397 *Science*, 92(4):497–501, 2007.
- 398 [17] J. Lopez, S. Oller, E. Onate, and J. Lubliner. A homogeneous constitutive model for masonry. *Int. J. Numer. Meth.*  
399 *Engng.*, 46:1651–1671, 1999.
- 400 [18] G. Magenes and G.M. Calvi. In-plane seismic response of brick masonry walls. *Earthquake Engineering and Structural*  
401 *Dynamics*, 26:1091–1112, 1997.
- 402 [19] C.S. Meisl, K.J. Elwood, and C.E. Ventura. Shake table tests on the out-of-plane response of unreinforced masonry  
403 walls. *Canadian Journal Civil Engineering*, 34:1381–1392, 2007.
- 404 [20] G. Milani. Simple homogenization model for the non-linear analysis of in-plane loaded masonry walls. *Computers*  
405 *and Structures*, 89:1586–1601, 2011.
- 406 [21] G. Milani. Simple lower bound limit analysis homogenization model for in-and out-of-plane loaded masonry walls.  
407 *Construction and Building Materials*, 25:4426–4443, 2011.
- 408 [22] G. Milani, K. Beyer, and A. Dazio. Upper bound limit analysis of meso-mechanical spandrel models for the pushover  
409 analysis of 2D masonry frames. *Engineering Structures*, 31:2696–2710, 2009.

- 410 [23] G. Milani, P. Lourenco, and A. Tralli. Homogenised limit analysis of masonry walls, part i: Failure surfaces.  
411 *Computers and Structures*, 84:166–180, 2006.
- 412 [24] G. Milani, P. Lourenco, and A. Tralli. 3D homogenized limit analysis of masonry buildings under horizontal loads.  
413 *Engineering Structures*, 29:3134–3148, 2007.
- 414 [25] G. Milani, P.B. Lourenco, and A. Tralli. Homogenised limit analysis of masonry walls, part ii: Structural examples.  
415 *Computers and Structures*, 84:181–195, 2006.
- 416 [26] G. Milani, E. Miani, and A. Tralli. Approximate limit analysis of full scale FRP-reinforced masonry buildings through  
417 a 3D homogenized fe package. *Composite Structures*, 92:918–935, 2010.
- 418 [27] J. Paquette and M. Bruneau. Pseudo- dynamic testing of unreinforced masonry building with flexible diaphragm.  
419 *Journal of Structural Engineering ASCE*, 129(6):708–716, 2003.
- 420 [28] J. Paquette and M. Bruneau. Pseudo- dynamic testing of unreinforced masonry building with flexible diaphragm. In  
421 *In: 13th World Conference on Earthquake Engineering Vancouver*, B.C., Canada, paper 2609, 2004.
- 422 [29] J. Paquette and M. Bruneau. Pseudo- dynamic testing of unreinforced masonry building with flexible diaphragm  
423 and comparison with existing procedures. *Construction and Building Materials*, 20:220–228, 2006.
- 424 [30] J. Park, P. Towashiraporn, J.I. Craig, and B.J. Goodno. Seismic fragility analysis of low-rise unreinforced masonry  
425 structures. *Engineering Structures*, 31:125–137, 2009.
- 426 [31] L. Pasticier, C. Amadio, and M. Fragiocomo. Non-linear seismic analysis and vulnerability evaluation of a masonry  
427 building by means of the sap2000 v.10 code. *Earthquake Engineering and Structural Dynamics*, 37:467–485, 2008.
- 428 [32] P. Roca. Assessment of masonry shear-walls by simple equilibrium models. *Construction and Building Materials*,  
429 20:229–238, 2006.
- 430 [33] M. Rota, A. Penna, and G. Magenes. A methodology for deriving analytical fragility curves for masonry buildings  
431 based on stochastic nonlinear analyses. *Engineering Structures*, 32:1312–1323, 2010.
- 432 [34] T. Salonikios, C. Karakostas, V. Lekidis, and A. Anthoine. Comparative inelastic pushover analysis pf masonry  
433 frames. *Engineering Structures*, 25:1515–1523, 2003.
- 434 [35] I. Sharif, C.S. Meisl, and K.J. Elwood. Assessment of asce 41 height-to-thickness ratio limits for urm walls. *Earthquake  
435 Spectra*, 23(4):893–908, 2007.
- 436 [36] M. Shariq, H. Abbas, H. Irtaza, and M. Qamaruddin. Influence of openings on seismic performance of masonry  
437 building walls. *Building and Environment*, 43:1232–1240, 2008.
- 438 [37] A. Tena-Colunga, A. Juarez-Angeles, and V.H. Salinas-Vallejo. Cyclic behavior of combined and confined masonry  
439 walls. *Engineering Structures*, 31:240–259, 2009.
- 440 [38] G. Vasconcelos and P.B. Lourenco. Experimental characterization of stone masonry in shear and compression.  
441 *Construction and Building Materials*, 23:3337–3345, 2009.